A new lock-step mechanism of matrix remodelling based on subcellular contractile events

Lysianne Follonier Castella[1,2], Lara Buscemi[1], Charles Godbout[1,2], Jean-Jacques Meister[1] and Boris Hinz[2,*]

[1]Laboratory of Cell Biophysics, Ecole Polytechnique Fédérale de Lausanne (EPFL), CH-1015 Lausanne, Switzerland
[2]Laboratory of Tissue Repair and Regeneration, Matrix Dynamics Group, Faculty of Dentistry, Fitzgerald Building, University of Toronto, 150 College Street, Toronto, ON M5S 3E2, Canada
*Author for correspondence (boris.hinz@utoronto.ca)

Accepted 5 March 2010
Journal of Cell Science 123, 1751-1760

doi:10.1242/jcs.066795

Summary

Myofibroblasts promote tissue contractures during fibrotic diseases. To understand how spontaneous changes in the intracellular calcium concentration, $[Ca^{2+}]_i$, contribute to myofibroblast contraction, we analysed both $[Ca^{2+}]_i$ and subcellular contractions. Contractile events were assessed by tracking stress-fibre-linked microbeads and measured by atomic force microscopy. Myofibroblasts exhibit periodic (~100 seconds) $[Ca^{2+}]_i$ oscillations that control small (~400 nm) and weak (~100 pN) contractions. Whereas depletion of $[Ca^{2+}]_i$ reduces these microcontractions, cell isometric tension is unaffected, as shown by growing cells on deformable substrates. Inhibition of Rho- and ROCK-mediated Ca^{2+}-independent contraction has no effect on microcontractions, but abolishes cell tension. On the basis of this two-level regulation of myofibroblast contraction, we propose a single-cell lock-step model. Rho- and ROCK-dependent isometric tension generates slack in extracellular matrix fibrils, which are then accessible for the low-amplitude and high-frequency contractions mediated by $[Ca^{2+}]_i$. The joint action of both contraction modes can result in macroscopic tissue contractures of ~1 cm per month.

Key words: Myofibroblast, Fibrosis, Calcium oscillations, Rho kinase, Stress fibre, Collagen

Introduction

Myofibroblasts are responsible for the excessive deposition and irreversible remodelling of the extracellular matrix (ECM) that hallmarks virtually all fibrotic diseases and impedes organ function, often leading to lethal organ failure (Wynn, 2008). In the heart, fibrosis is associated with a variety of severe conditions, including rheumatic disease, pathological hypertrophy, cardiomyopathy and post-myocardial infarct remodelling (Kahan et al., 2009; Lazzerini et al., 2006). Following myocardial injury (e.g. after infarct) or in response to increased mechanical load (e.g. during hypertension), myofibroblasts can derive from different precursor cells, including local cardiac fibroblasts. The fibroblast to myofibroblast transition occurs in response to transforming growth factor β1 (TGFβ1) and heightened tension in the extracellular environment (Tomasek et al., 2002; Wipff and Hinz, 2008). Myofibroblasts are primarily characterised by neo-expression of α-smooth muscle actin (α-SMA) in stress fibres, where it associates with non-muscle myosin II, thus increasing their contractility (Hinz et al., 2001). During myofibroblast differentiation, fibroblastic cells lose their migratory phenotype and become sessile (Ronnov-Jessen and Petersen, 1996). This switch is promoted by the formation of large focal adhesions (FAs) that enable strong attachment between intracellular stress fibres and ECM proteins such as collagen and fibronectin (FN) (Hinz et al., 2003). Strong contraction and adhesion enable the myofibroblast to remodel tissues even against the considerable stress arising during tissue remodelling (Hinz, 2009; Wang et al., 2006).

Myofibroblast contraction might result in irreversible tissue contractures over days, months and even years (Tomasek et al., 2002). However, the mode and regulatory mechanisms of this process at the single-cell level remain elusive. The persisting character of myofibroblast contraction has suggested that α-SMA stress-fibre contraction is predominantly regulated by inhibition of myosin light chain (MLC) phosphatase (MLCP) mediated by Rho and Rho-associated kinase (ROCK). This would be similar to the regulation of fibroblast contraction (Katoh et al., 2001b; Tomasek et al., 2002). Other reports have maintained that myofibroblast contraction is regulated by changes in intracellular Ca^{2+} concentration ($[Ca^{2+}]_i$) and MLC kinase (MLCK) (Follonier et al., 2008; Furuya et al., 2005; Goto et al., 1998; Levinson et al., 2004; Raizman et al., 2007), which is well described for phenotype-related smooth muscle cells (SMCs) (Kamm and Stull, 1989).

Here, we set out to elucidate the contributions of intracellular Ca^{2+} concentration, $[Ca^{2+}]_i$, and Rho and ROCK signalling to the regulation of myofibroblast contraction. We have previously shown that cultured myofibroblasts exhibit spontaneous $[Ca^{2+}]_i$ oscillations that are coordinated between contacting cells (Follonier et al., 2008). Our observations suggested that $[Ca^{2+}]_i$ oscillations and myofibroblast contractile activity are mechanistically linked (Follonier et al., 2008). We investigate whether periodic $[Ca^{2+}]_i$ transients give rise to subsequent contractile events at the subcellular level by analysing: $[Ca^{2+}]_i$ variations using fluorescence imaging; subcellular contractions using high-resolution tracking of stress-fibre-coupled microbeads and force/displacement measurements with atomic force microscopy (AFM); and myofibroblast isometric tension using deformable silicone culture substrates. We show that myofibroblasts exhibit cyclic and rapid microcontractile events of ~400 nm that are correlated with periodic $[Ca^{2+}]_i$ oscillations. Concomitantly, myofibroblasts are able to maintain isometric tension in a Rho- and ROCK-dependent mechanism. We present a lock-step model of myofibroblast remodelling that explains how both contraction mechanisms collaborate to produce tissue contracture.

Journal of Cell Science

Results

Culture on 'remodelling-tissue-compliant' substrates produces the myofibroblast phenotype

To mimic pathophysiologically relevant mechanical conditions of connective tissue undergoing remodelling (Goffin et al., 2006), we routinely cultured cardiac fibroblasts on silicone substrates with a Young's modulus of 15 kPa. In standard culture, ~90% of cardiac fibroblasts spontaneously develop the myofibroblast phenotype. We first compared formation of α-SMA stress fibres in cells cultured on 15 kPa substrates with that in cells cultured on glass coverslips (Fig. 1). In both conditions, early-passage myofibroblasts (P1-P3) developed comparable morphologies (Fig. 1A) and similar percentages of cells exhibiting α-SMA in stress fibres (~90%) (Fig. 1B). In later passages (P4-P5), the percentage of cells positive for α-SMA stress fibres significantly decreased on 15 kPa substrates (~65%) compared with glass coverslip controls (~85%) (Fig. 1B). As described earlier (Goffin et al., 2006), α-SMA shifted to a cytosolic localisation in 35% of cells cultured on soft substrates (Fig. 1A, arrowhead). Therefore, all the following experiments were performed between passages 1 to 3. In selected experiments, we used specialised 15 kPa silicone substrates that 'wrinkle' upon exertion of high cell forces (Fig. 1C) (Hinz et al., 2001).

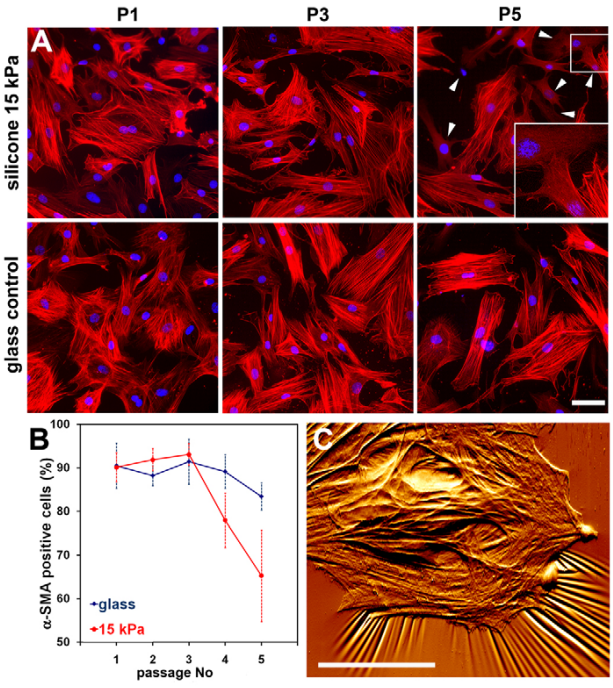

Fig. 1. Cardiac fibroblasts differentiate into myofibroblasts on 15 kPa substrates. (**A**) Cardiac fibroblasts from passages P1 to P5 were cultured on 15 kPa soft silicone substrates and on control glass coverslips, both coated with 10 μg/ml collagen I. After 4 days, cells were immunostained for myofibroblast marker α-SMA (red) and cell nuclei (blue). Cells with cytosolic as opposed to stress-fibre localisation of α-SMA are indicated by arrowheads. (**B**) The percentages of cells positive for stress-fibre localisation of α-SMA were quantified for every passage on each substrate. Mean values (± s.d.) were calculated from five independent experiments. (**C**) On 15 kPa silicone substrates, myofibroblasts generated wrinkles in the surface, as visualised by AFM in imaging mode. Scale bars: 50 μm.

Cardiac myofibroblasts exhibit spontaneous Ca^{2+} oscillations

One objective of our study was to relate contractile events in myofibroblasts to periodic changes in $[Ca^{2+}]_i$. We have recently shown that rat subcutaneous myofibroblasts exhibit spontaneous $[Ca^{2+}]_i$ oscillations in standard culture (Follonier et al., 2008). Here, we loaded cardiac myofibroblasts with the Ca^{2+} indicator Fura-2 and recorded time-lapse sequences of fluorescence images over 10-40 minutes. The $[Ca^{2+}]_i$ fluorescence ratio was calculated for every cell and plotted over time (Fig. 2A). We observed periodic $[Ca^{2+}]_i$ oscillations in ~42% of analysed cells and determined the dominant oscillation frequency for every cell by fast Fourier transform analysis. From the histogram shown in Fig. 2B, a main period of 99±32 seconds was determined for 87% of the cells; a second maximum indicated a longer period of 221±21 seconds for 13% of the cells. Cells in the latter population fulfilled the morphological criteria of α-SMA-negative fibroblasts, with a smaller spreading area compared with myofibroblasts.

Agonists that modulate cell contraction and/or Ca^{2+} signalling were first tested for their effect on the spontaneous $[Ca^{2+}]_i$ oscillations (Fig. 2C). Addition of the ROCK inhibitor Y27632 (10 μM) did not cause any substantial change in the frequency and amplitude of $[Ca^{2+}]_i$ oscillations (Fig. 2C, green profile). Extracellular ATP, previously described to stimulate $[Ca^{2+}]_i$ signalling in fibroblastic cells by means of a G-protein-coupled receptor (Grierson and Meldolesi, 1995), increased the $[Ca^{2+}]_i$ oscillation frequency by approximately 30% without impacting the amplitude when applied in a defined range of low concentrations (10-100 nM) (Fig. 2C, blue profile). At higher concentrations, the addition of ATP resulted in one high $[Ca^{2+}]_i$ transient and terminated the oscillatory behaviour (our unpublished data). To reduce the $[Ca^{2+}]_i$ level and to abolish $[Ca^{2+}]_i$ oscillations, we tested different approaches. Chelation of Ca^{2+} in the extracellular medium using EGTA (3 mM) mildly reduced the $[Ca^{2+}]_i$ oscillation frequency over 30 minutes (our unpublished data), demonstrating the role of intracellular Ca^{2+} stores in periodic oscillations. Thapsigargin, an inhibitor of the endoplasmic reticulum Ca^{2+}-ATPase, first induced a rapid release of Ca^{2+} from intracellular stores. Store depletion leads to activation of Ca^{2+}-permeable channels in the plasma membrane and constitutively sustained $[Ca^{2+}]_i$ in lung and cardiac fibroblasts (Chen et al., 2010; van Rossum et al., 2000), as well as in our cardiac myofibroblasts (Fig. 2C, red profile). By adding 2-aminoethoxydiphenyl borate (2-APB) during the thapsigargin-induced Ca^{2+} entry phase, we achieved a rapid drop in $[Ca^{2+}]_i$ to baseline (Fig. 2C, red profile), similar to what was previously described in SMCs (van Rossum et al., 2000). 2-ABP has been suggested to act as an inositol (1,4,5)-trisphosphate [Ins(1,4,5)P_3] receptor and/or store-operated channel blocker (Bootman et al., 2002; Chen et al., 2010). 2-APB alone was only efficient in completely removing intracellular Ca^{2+} when cardiac myofibroblasts were kept in a Ca^{2+}-free medium but not in a Ca^{2+}-containing medium (our unpublished data); this confirms previous data on normal rat kidney fibroblasts (Harks et al., 2003). Because extracellular Ca^{2+} is important for effective integrin binding to ECM proteins, a crucial element in our experiments, we always used a combination of thapsigargin and 2-APB to deplete intracellular Ca^{2+}.

ECM-coated microbeads reveal subcellular contractions when coupled to stress fibres

A dramatic and sustained increase in $[Ca^{2+}]_i$ has been shown to induce whole-cell contraction of myofibroblasts (Follonier et al.,

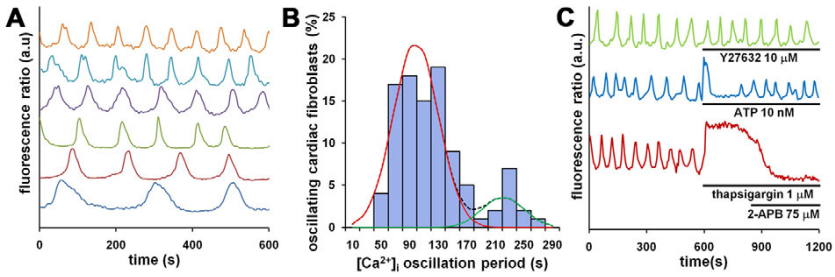

Fig. 2. Myofibroblasts exhibit spontaneous periodic $[Ca^{2+}]_i$ oscillations. (**A**) The Em340/Em380 fluorescence ratios of Fura-2-loaded cells were recorded every 5 seconds over ROI including individual myofibroblasts and plotted over time. (**B**) The dominant periods of $[Ca^{2+}]_i$ oscillations were determined by fast Fourier transform of each profile and summarised in a histogram (N_{cells}=100, $n_{experiments}$=35). Gaussian fitting of the histogram (red and green lines) and overall fitting by least-squares fit to the Gaussian functions (dashed line) revealed two maxima at 99 seconds, including 87% of all cells, and 221 seconds, including 13% of all cells. (**C**) Fura-2-loaded myofibroblasts were treated with different drugs to assess their effects on spontaneous $[Ca^{2+}]_i$ oscillations. ROCK was inhibited by adding 10 μM Y27632, $[Ca^{2+}]_i$ was depleted by combining 1 μM thapsigargin and 75 μM 2-APB, and $[Ca^{2+}]_i$ oscillations were stimulated with 10 nM ATP. Fura-2 Em340/Em380 ratios are displayed for one representative cell per condition.

2008; Furuya et al., 2005; Goto et al., 1998), but the role of periodic and short $[Ca^{2+}]_i$ oscillations is virtually unknown. To quantify possible subcellular contractile events, we tracked the movement of collagen- and FN-coated microbeads on the surface of cardiac myofibroblasts. ECM-coated 1 μm diameter beads recruited the FA marker vinculin and promoted coupling with stress fibres on the dorsal cell surface within 10-30 minutes (Fig. 3A, arrowheads). We then transiently transfected myofibroblasts with α-SMA–EGFP and performed combined phase-contrast (beads) and fluorescence (α-SMA stress fibres) video microscopy (Fig. 3B). The resulting time-lapse sequences demonstrated that a significant fraction of beads colocalised with stress fibres during their overall centripetal movement. Bead motility appeared to be promoted by contraction and displacement of the whole stress fibre as opposed to processive walking along the fibre (Fig. 3B, arrowheads).

To quantify the movement of ECM-coated beads on the dorsal surface of cardiac myofibroblasts, we analysed phase-contrast image sequences with particle-tracking software. To exclude cell-motility-related phenomena (Schmidt et al., 1993), we did not consider beads in the 10 μm lamellipodial region of the cell periphery. The obtained *x*/*y* bead tracks could be classified into three different behaviours: directed, diffusive and immobile (Fig. 3C). This classification was automated by means of a custom-made algorithm that set criteria on the velocity and the diffusion coefficient of beads (supplementary material Fig. S1). Of all analysed beads on untreated cells, 53% displayed directed motion, 31% were diffusive and 16% were immobile (Fig. 3D, pie chart). The mean velocity of directed moving beads under control conditions was 4.3±2.7 nm/s (15 μm/hour) (Fig. 3D, histogram). To verify that directed bead movements were generated by active contraction, we blocked the ATPase activity of myosin II using 50 μM blebbistatin (Fig. 4A). Blebbistatin completely abolished directed bead movement in ~50% of cases and reduced movement in the rest. FA and stress-fibre association with beads and substrate was preserved at 50 μM (supplementary material Fig. S2). Statistical evaluation of beads with directed motion revealed an approximately twofold decrease in average bead velocity after blebbistatin treatment to 1.9±1.4 nm/s, indicated by the shortening to 0.5±0.3 of the relative vector $\overline{\mathbf{V}}_{blebbistatin}$ compared to the control vector $\mathbf{V}_{control}$ (length=1) in a polar plot (Fig. 4A). These results show that microbead movements are indicative of subcellular contractions promoted by stress fibres on the dorsal cell surface. In all following experiments, we restricted our analysis to beads with directed, that is, contraction-driven, motion.

Because myofibroblasts were cultured on wrinkling silicone substrates (Young's modulus of 15 kPa), we could simultaneously assess isometric tension development at the whole-cell level. Under control conditions, myofibroblast isometric contraction generated substrate wrinkles that were perpendicular to the axis of stress fibre orientation and were stable over several hours of observation (Fig. 1C; Fig. 4). Cell behaviour was monitored using phase-contrast microscopy for a minimum of 20 minutes before and for 30-60 minutes after treatment with drugs (Fig. 4). In addition to blocking subcellular contraction and microbead movement, blebbistatin completely inhibited isometric tension production, as seen from wrinkle disappearance within 20 minutes of treatment (Fig. 4A). The elastic recoil of the wrinkled substrate generated a passive 'backward' movement in ~50% of the beads on the same cells with respect to their control 'forward' direction (Fig. 4A). This direction change contributed to the average deviation from the control vector direction of $\Delta\theta_{blebbistatin}$=84±68° (Fig. 4A).

ECM-coated bead motion is driven by $[Ca^{2+}]_i$, whereas isometric cell tension depends on ROCK

Next, we applied our setup to decipher the role of $[Ca^{2+}]_i$ in both modes of contraction. Complete depletion of $[Ca^{2+}]_i$ using a combination of thapsigargin and 2-APB (Fig. 2C) decreased bead velocity within 20 minutes ($\overline{V}_{thapsi\text{-}2\text{-}APB}$=0.7±0.3) (Fig. 4B). Bead direction remained largely unchanged ($\Delta\theta_{thapsi\text{-}2\text{-}APB}$=16±19°) and stress-fibre connection through FAs was not affected (supplementary material Fig. S2). Importantly, $[Ca^{2+}]_i$ depletion did not affect isometric cell tension, as demonstrated by the maintenance of wrinkles during the entire experiment (Fig. 4B). We conclude that $[Ca^{2+}]_i$ regulates subcellular contractions of dorsal stress fibres connected to unrestrained microbeads, but not isometric contraction of ventral stress fibres engaged with the mechano-resistant elastic substrate.

To test whether isometric tension is regulated by Rho and ROCK, we treated cardiac myofibroblasts with the ROCK inhibitor Y27632, which induced relaxation of stress fibres and loss of substrate wrinkles within 25 minutes (Fig. 4C). During the phase

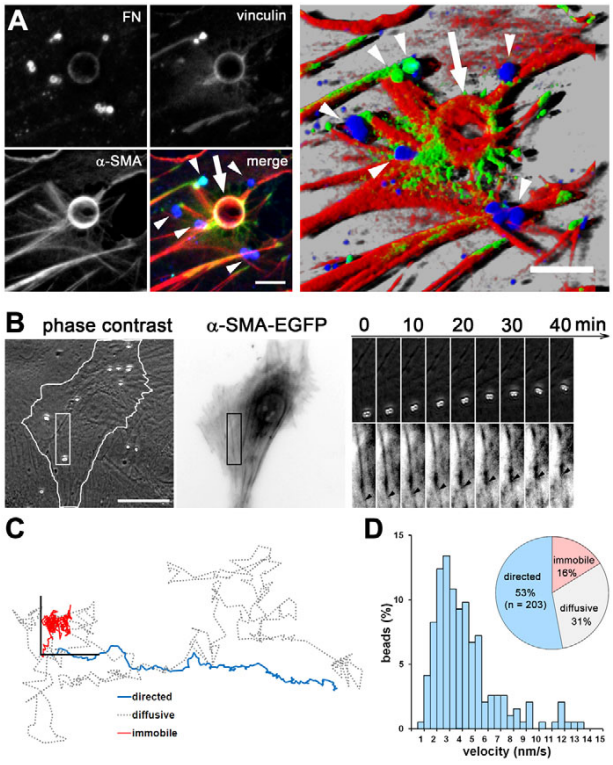

Fig. 3. Tracking of ECM-coated microbeads reveals subcellular stress-fibre contractions. (**A**) Microbeads of 1 μm (arrowheads) and 5 μm (arrow) diameter were seeded for 10 minutes on the surface of cultured myofibroblasts. Samples were immunostained for α-SMA (red, stress fibres), vinculin (green, FAs) and FN (blue, beads). Confocal imaging, deconvolution and subsequent 3D reconstruction in a shadow projection demonstrate that beads connect to stress fibres on the dorsal cell surface by promoting the formation of FAs. Scale bars: 5 μm. (**B**) Sequences of phase-contrast images of myofibroblasts (cell outlined) were used to track bead motion. Simultaneous recording of inverted fluorescence images of α-SMA–EGFP-transfected myofibroblasts was used to follow stress-fibre dynamics. A substantial fraction of beads colocalised with stress fibres and followed their contraction. Arrowheads indicate bead positions that, over time, colocalise with a phase dense spot on the stress fibre. Scale bar: 30 μm. (**C**) The positions of three example beads were tracked for 20 minutes every 5 seconds and displayed in an *x*/*y* plot (axis length=1 μm), illustrating the typical modes of motion: directed, diffusive and immobile. (**D**) A custom-made algorithm (supplementary material Fig. S1) was used to classify bead behaviour, summarised in the pie chart ($n_{experiments}$=27, N_{beads}=383). The mean velocities of the directed moving beads are summarised in the histogram ($N_{directed\text{-}beads}$=203).

of wrinkle relaxation (Fig. 4C, 24-48 minutes), bead movement stopped or was reversed. Akin to blebbistatin treatment, bead backward movement was passively driven by relaxation of the elastic substrate. After substrate recoil, beads resumed moving with their original velocity and direction. It should be noted that wrinkles did not reappear, indicating that ROCK-mediated isometric contraction was still inhibited while beads continued to move. Formation of ventral and dorsal stress fibres was not affected during the experiment at the given drug concentration (supplementary material Fig. S2). Bead behaviour is exemplified for one experiment in *x*/*y* tracks (Fig. 4C) and summarised for all experiments in a polar plot (Fig. 4C). On average, bead velocity remained unchanged by ROCK inhibition (∇_{Y27632}=1.0±0.6) and bead direction deviated by $\Delta\theta_{Y27632}$=65±70°, because of the transient phase of backward movement. Taken together, these results suggest that two modes of contraction operate simultaneously in cultured cardiac myofibroblasts: isometric cell tension is regulated by Rho and ROCK signalling, and is apparently insensitive to periodic oscillations and experimental depletion of $[Ca^{2+}]_i$, whereas contractile forces exerted on ECM-coated microbeads require only $[Ca^{2+}]_i$.

Periodic $[Ca^{2+}]_i$ oscillations correlate with microcontractile events of dorsal stress fibres

To investigate whether the periodic $[Ca^{2+}]_i$ oscillations observed in cardiac myofibroblasts are related to periodic microcontractile events, we simultaneously analysed $[Ca^{2+}]_i$ variations, using fluorescence imaging, and microcontractions, using tracking of stress-fibre-coupled beads in phase-contrast images (Fig. 5). When analysed with high spatial resolution, beads moved in a stepwise fashion, because they exhibited alternating phases of rapid movement and stationary behaviour. The step amplitude varied between 200 and 1000 nm, with an average of 400±200 nm. The time intervals between step onsets were time correlated with periods of $[Ca^{2+}]_i$ transients. During one $[Ca^{2+}]_i$ transient (Fig. 5A, dashed lines, ~100 seconds), we detected one bead step (60%), two steps (30%) or no step (10%). To quantify the relationship between both signals, we measured the time lag between every $[Ca^{2+}]_i$ peak and step onset (Fig. 5A, arrowheads) occurring during each transient. In 70% of cases, onset of a first step (Fig. 5B, dark grey bars) was detected during the $[Ca^{2+}]_i$ increase, 10-30 seconds after the start of the $[Ca^{2+}]_i$ transient. First steps preceded the $[Ca^{2+}]_i$ peak (but not the Ca^{2+} increase) with two maxima at –30 seconds and –10 seconds (Fig. 5B). If a second step occurred, it was always initiated after the $[Ca^{2+}]_i$ peak, with a maximum at 20 seconds in the histogram (Fig. 5B, light grey bars). Our findings suggest that $[Ca^{2+}]_i$ variations control myofibroblast subcellular contraction by inducing cyclic and rapid microcontractions.

Finally, we set out to determine the forces of the microcontractions that follow single $[Ca^{2+}]_i$ transients using combined fluorescence microscopy and real-time AFM. We used 5 μm diameter glass spheres attached to the tip of an AFM force probe (Fig. 6A). ECM-coated 5 μm beads recruited dorsal stress fibres at sites of FAs within 10 minutes (Fig. 3A, arrow). The spherical AFM tip was brought into contact with a Fluo-4-loaded myofibroblast selected for spontaneous $[Ca^{2+}]_i$ oscillations (Fig. 6B). The applied contact force of 250 pN induced no detectable changes in the $[Ca^{2+}]_i$ oscillation period (our unpublished data). Contact was maintained for at least 10 minutes to ensure signal stability and attachment of the ECM-coated probe to stress fibres. By simultaneously recording $[Ca^{2+}]_i$ oscillations and vertical deflections of the AFM force probe, we established a relationship between $[Ca^{2+}]_i$ and microcontractile pulling events (Fig. 6C, force increase) over time. The periodic pulling events were phase shifted by 30-60 seconds with respect to the oscillating Ca^{2+} transients (Fig. 6C), similar to the Ca^{2+} transient and bead step time relationship. Under control conditions, microcontractile events induced a mean probe displacement of 10-20 nm, corresponding to a mean force of 104±89 pN. Their main periodic occurrence – every 116 seconds (frequency of 8.6 mHz) – closely matched that

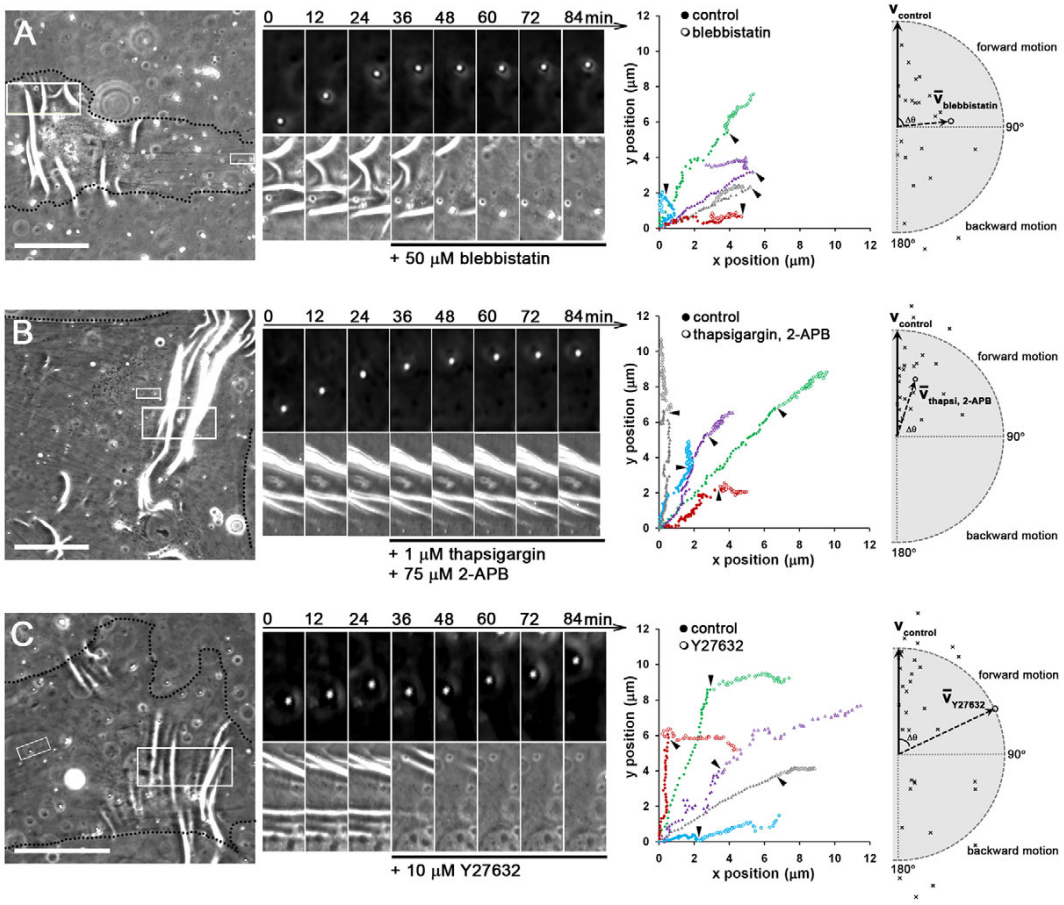

Fig. 4. Subcellular contractions are $[Ca^{2+}]_i$ dependent, whereas isometric cell tension is regulated by ROCK. Microbeads were seeded for 30 minutes on the surface of myofibroblasts cultured on wrinkling 15 kPa substrates. Cells were treated with (**A**) the myosin II inhibitor blebbistatin (50 µM), (**B**) thapsigargin (1 µM) and 2-APB (75 µM) to deplete $[Ca^{2+}]_i$, and (**C**) the ROCK inhibitor Y27632 (10 µM). Sequences of phase-contrast images were recorded for 24 minutes under control conditions, followed by 60 minutes of drug treatment. The cell outline is indicated by a dotted line. Drug effects were evaluated for contraction-driven bead movement (small ROI, top image series) and wrinkle formation by isometric cell contraction (large ROI, bottom image series). Bead tracks of one representative experiment are displayed in *x*/*y* graphs; filled symbols indicate 20 minutes of control recording and empty symbols indicate 20 minutes of recording after addition of drugs. To statistically express drug effects on bead movement, we calculated the ratio of the mean bead velocity before and after drug treatment, $V_{drug}/V_{control}$, for every directed moving bead; the same was done for the angle of bead direction change, $\Delta\theta=|\theta_{drug}-\theta_{control}|$. In a polar plot, the relative velocity (distance from origin) and direction (angle position from vertical control, $\Delta\theta$) were displayed for all beads (single data points). The average bead behaviour was summarised as the mean vector ($\overline{V}_{drug}$) relative to the control vector, $V_{control}$, with velocity=1 and $\theta=0°$. Beads displayed in the upper quadrant maintained direction ('forward'), whereas beads in the lower quadrant moved 'backward' after drug addition. Data points outside the half circle belong to beads that increased speed after stimulation. Some data points are out of range for display, but were considered in the analysis. Blebbistatin: $n_{experiments}=5$, $N_{beads}=26$; thapsigargin and 2-APB: $n_{experiments}=3$, $N_{beads}=18$; and Y27632: $n_{experiments}=11$, $N_{beads}=40$. Scale bars: 50 µm.

of the oscillating $[Ca^{2+}]_i$ transients, as seen in histograms produced from fast Fourier analysis (Fig. 6D). To test whether correlation persisted after challenging the system, we increased the frequency of $[Ca^{2+}]_i$ oscillations with 10 nM ATP, as described elsewhere (Grierson and Meldolesi, 1995). Addition of ATP reduced the main $[Ca^{2+}]_i$ period from 116 seconds to 80 seconds (12.5 mHz) and concomitantly reduced the main period of microcontractile events to 75 seconds (13.3 mHz) (Fig. 6D). ATP did not produce a significant change in the force amplitude.

Discussion

Myofibroblasts produce the irreversible tissue contractures characteristic of organ fibrosis; however, it remains controversial how myofibroblast contractile activity is regulated on the cellular level. Here, we assessed isometric tension development and subcellular contractile events in the same cell, using an experimental setup that recapitulates aspects of (visco-)elastic ECM bulk behaviour and local ECM fibril transport (Fig. 7). Our results show that two modes of contraction cooperate in the same myofibroblast through differently regulated pathways. Maintenance of isometric tension against a mechanically opposing substrate is controlled by Rho and ROCK, and is unaffected by $[Ca^{2+}]_i$ depletion. Conversely, periodic contractile forces exerted on unrestrained ECM-coated beads on the myofibroblast surface are governed by spontaneous $[Ca^{2+}]_i$ oscillations and are insensitive to ROCK inhibition.

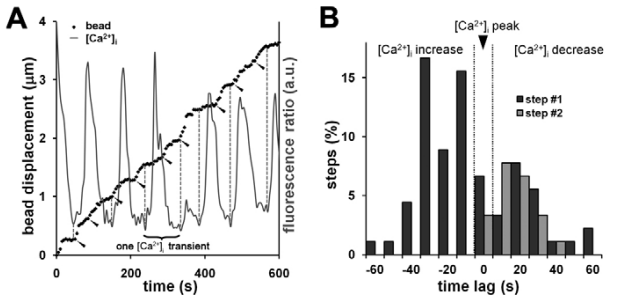

Fig. 5. $[Ca^{2+}]_i$ oscillations correlate with cyclic subcellular contractions of stress fibres. (**A**) $[Ca^{2+}]_i$ variations and contraction-driven displacement of beads on the dorsal cell surface were simultaneously analysed. The Fura-2 fluorescence ratio of one representative myofibroblast was recorded every 5 seconds, together with bead movement in phase-contrast images. $[Ca^{2+}]_i$ variations and bead displacement were compared on a relative scale over time. Beads are typically characterised by stepwise movements; each step onset is indicated by an arrowhead. Dashed lines connect every initiation of a $[Ca^{2+}]_i$ transient with the bead displacement curve. (**B**) The degree of coupling between both signals was quantified by measuring the lag time between every $[Ca^{2+}]_i$ peak (N_{Ca2+}=80, $n_{experiments}$=8) and onset of the associated first step (N_{step1}=68) or sometimes second step (N_{step2}=22) occurring during the transient. All lag times were summarised in a histogram, showing first (dark grey columns) and second (light grey columns) step separately. A negative time lag means that step initiation occurred during the phase of $[Ca^{2+}]_i$ increase; a positive time lag indicates that step initiation followed the $[Ca^{2+}]_i$ peak.

From these findings, we propose a single-cell lock-step mechanism for long-term tissue contractures (Fig. 7). Strong Rho- and ROCK-mediated isometric cell contraction generates slack in individual collagen fibrils. Such stress-released fibrils are pulled in by periodic $[Ca^{2+}]_i$-dependent microcontractions until fibril tension is restored. Locally contracted fibrils can be proteolytically processed and/or stabilised by addition of new ECM material and new crosslinks. Once remodelled, the fibres can again carry mechanical load and cells are able to re-spread while the ECM remains shortened. Multiple iterations of this cycle will result in incremental and irreversible tissue contracture. Our tracking of unrestrained beads demonstrated microcontractile events with ~400 nm displacements that occur approximately every 100 seconds, resulting in a mean transport velocity of ~15 µm/hour. Translated to the tissue level, this could lead to shortening of around 1 cm per month, which is in the range of deformations observed in connective tissue contractures (Tomasek et al., 2002).

One novel finding is that cyclic microcontractile events directly correlate with periodic $[Ca^{2+}]_i$ oscillations. In fibroblastic cells, single $[Ca^{2+}]_i$ increases lead to contractile responses within tens of seconds after chemical and mechanical stimulation (Follonier et al., 2008; Munevar et al., 2004). Our results support the existence of a similar cause-effect relationship in myofibroblasts. Suppressing $[Ca^{2+}]_i$ oscillations eliminates microcontractions; increasing $[Ca^{2+}]_i$ oscillation frequency increases microcontraction frequency. Periodic $[Ca^{2+}]_i$ oscillations with comparable frequencies have been reported to occur in different cultured fibroblasts after various stimuli (Arora et al., 1994; Chen et al., 2010; Diliberto et al., 1994; Harootunian et al., 1991; Liang et al., 2003; Ridefelt et al., 1995; Uhlen et al., 2006; Wu et al., 2004); however, cell contractile events were not assessed in these studies. Rhythmic cortical pulsations were described for fibroblasts in suspension (Salbreux et al., 2007) and for spreading fibroblasts after microtubule depolymerisation – in the latter case, preceded by $[Ca^{2+}]_i$ transients (Pletjushkina et al.,

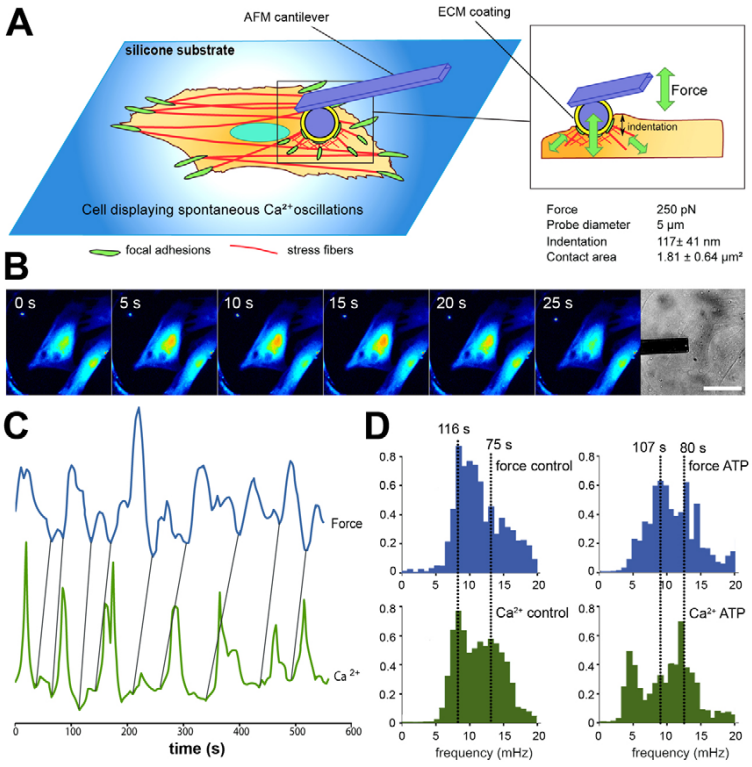

Fig. 6. AFM reveals that periodic $[Ca^{2+}]_i$ oscillations correlate with microcontractile events. (**A**) To simultaneously record $[Ca^{2+}]_i$ oscillations and microcontractile events of myofibroblast stress fibres, we used ECM-coated 5 µm glass beads attached to the tip of an AFM force probe (cantilever). (**B**) Time-lapse sequence of fluorescence images recorded for Fluo-4-loaded myofibroblasts (heat coloured) in contact with the AFM cantilever (bright field). Scale bar: 50 µm. (**C**) A representative simultaneously acquired $[Ca^{2+}]_i$ oscillation (green) and vertical force probe deflection (blue) is shown on a relative scale over time. Force curves are oriented to display cell pulling on the force probe as force increases (peaks); vertical lines show temporal correlation with the $[Ca^{2+}]_i$ signal. (**D**) The frequencies of $[Ca^{2+}]_i$ and force oscillations revealed matching of the dominant frequencies of both signals. The increase in the $[Ca^{2+}]_i$ oscillation frequency observed after the addition of ATP (10 nM) is associated with a corresponding increase in the force frequencies.

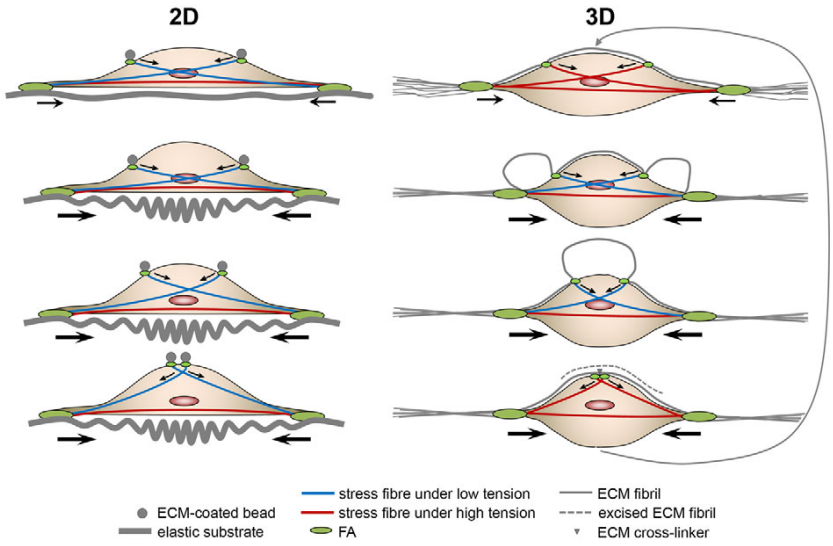

Fig. 7. Lock-step mechanism of ECM remodelling. ROCK-regulated isometric tension is exerted by ventral stress fibres, which have both ends engaged with the substrate at sites of FAs (green). On 2D elastic and deformable substrates, wrinkles are formed and maintained as the tension mounts (large arrows). By contrast, ECM-coated beads (grey circles) link to the free ends of dorsal stress fibres by creating a small FA and are pulled towards the cell centre. This movement is driven by the shortening of dorsal stress fibres, which experience less tension (blue, low tension) than the ventral stress fibres (red, high tension). Low-tension contraction is mediated by $[Ca^{2+}]_i$ oscillations. In a 3D environment, stress fibres are connected to ECM fibrils (grey) through FAs and keep the partially remodelled ECM under tension. ROCK-mediated global cell contraction (red stress fibres) shortens the bulk ECM and generates slack in individual ECM fibrils (grey loops). Such locally relaxed fibrils are now free to be contracted in a $[Ca^{2+}]_i$-dependent manner by low-tension stress fibres (blue). Incremental pulling events gradually shorten and stress the ECM fibrils. Local proteolytic processing and stabilisation of the fibrils by new ECM material and/or crosslinking (grey triangle) mechanically stabilise the remodelled ECM. Then, the cell can spread again to start a new cycle and the ECM remains shortened.

2001). We previously reported increasing $[Ca^{2+}]_i$ oscillation frequency during TGFβ1-induced differentiation of subcutaneous fibroblasts into highly contractile myofibroblasts (Follonier et al., 2008). Concomitantly, we measured slower oscillations in ~15% of cardiac myofibroblasts, which corresponds to the fraction of α-SMA-negative fibroblasts in the population. It is conceivable that a higher frequency of microcontractions is at least partly responsible for the higher efficiency of myofibroblasts to contract tissue.

What is the motor of microcontractile forces in cultured myofibroblasts? In migrating and spreading cells, collagen fibrils and ECM-coated microparticles are transported on the surface of lamellae, driven by periodic contractions and/or polymerising actin (Schmidt et al., 1993; Sheetz et al., 1989; Vogel and Sheetz, 2009); this process depends on MLCK activity (Giannone et al., 2004). Similar lamellipodial protrusion and retraction cycles participate in local pulling of collagen fibrils when fibroblasts are spread in or on newly polymerised 3D collagen gels (Meshel et al., 2005). This was shown to be largely independent of Rho and ROCK, although the role of spontaneous $[Ca^{2+}]_i$ oscillations was not assessed in these studies (Petroll et al., 2008; Tamariz and Grinnell, 2002). Several facts underline that the contractile forces in our experiments differ from motile events and rely on stress-fibre contraction. First, differentiated myofibroblasts are well-spread and essentially non-migratory cells. Second, we concentrated on microcontractile events several micrometres away from the cell periphery. Third, microbeads and AFM spherical tips clearly connected to stress fibres. Fourth, the bundled arrangement of the actin-myosin system in α-SMA stress fibres substantially differs from the cortical and highly dynamic arrangement at the cell periphery (Dugina et al., 2009; Pellegrin and Mellor, 2007). Consistently, lamellipodial protrusion and retraction cycles and membrane pulsations occur with higher frequency (~1-5/minute) and retractions are faster (2-5 μm/minute) (Meshel et al., 2005; Pelling et al., 2007) than the stress-fibre contractions in our myofibroblasts (~0.5/minute and 0.25 μm/minute).

Another central finding of our study is that the generation of periodic microcontractions and high tension occurs concurrently, but is regulated separately within the same myofibroblast. Microcontractions of myofibroblast stress fibres develop forces in the range 50-600 pN. This appears adequate to transport particles and bend collagen fibrils against moderate mechanical resistance (e.g. our elastic AFM force probe), but is not sufficiently strong to act against the high stress of tissue undergoing remodelling. Indeed, myofibroblasts transmit stresses of ~12 nN/μm^2 at sites of cell-ECM adhesions and develop forces of 4-8 μN on the whole-cell level, as measured by growth on deformable 'fibrosis-stiff' substrates (Goffin et al., 2006; Hinz et al., 2001; Wrobel et al., 2002). We show that the forces required to provide high isometric tension are predominantly regulated by Rho and ROCK, and are not affected by depleting cells of Ca^{2+}. Because weak microcontractions and strong global contraction are both promoted by stress fibres, the question arises as to what determines the mode of contraction. Formation and maintenance of stress fibres in the central region of cultured fibroblasts were shown to be sensitive to Rho and ROCK inactivation of MLCP, whereas peripheral stress fibres required $[Ca^{2+}]_i$ and MLCK activity (Katoh et al., 2001a; Totsukawa et al., 2000). Another regional and functional distinction has been made between dorsal and ventral stress fibres of cells

grown on 2D substrates (Hotulainen and Lappalainen, 2006; Pellegrin and Mellor, 2007). Moreover, the subcellular distribution of myosin isoforms IIA and IIB might influence local versus global regulation of contraction (Cai et al., 2006). One important difference between these stress-fibre populations is the level of applied stress. It is tempting to speculate that (dorsal) fibres under low tension, such as those connected to unrestrained microbeads, highly flexible AFM force probes or free-moving collagen fibrils, are particularly responsive to $[Ca^{2+}]_i$ changes. Conversely, (ventral) stress fibres under high tension, such as those pulling on a non-deformable coverslip or contracting an elastic substrate or stiff scar ECM, would predominantly employ the Rho and ROCK pathway. Consistently, isolated stress fibres have the intrinsic capability to respond to both Ca^{2+}-MLCK and Rho-ROCK-MLCP regulation (Katoh et al., 2001b).

Until now, Rho- and ROCK-regulated inhibition of MLCP has been considered the major pathway controlling tissue contraction by myofibroblasts (Tomasek et al., 2002). Indeed, contraction of myofibroblast-populated wound granulation tissue and restrained collagen gels is affected by Rho, ROCK and MLCP modulation, but less so by $[Ca^{2+}]_i$ effectors (Parizi et al., 2000; Tomasek et al., 2006). These acute and multicellular experimental setups would not detect the small and weak contractions following single $[Ca^{2+}]_i$ transients. However, the iterative nature of these contractions can add up to steady shortening of the ECM in the long term. According to our model, this will only function if a Rho- and ROCK-mediated strong and longer-lasting contraction previously generated slack in ECM fibrils. We conclude that both contraction modes are coordinated and required to promote slow and irreversible shortening of connective tissue in fibrosis.

Materials and Methods

Cell culture and reagents

Primary cardiac fibroblasts were explanted from rat heart ventricles. Cultures were systematically tested for fibroblast purity by immunostaining for the fibroblast marker vimentin and the absence of the SMC marker desmin and the endothelial cell markers von Willebrand factor, PECAM-1 and VE-cadherin. After culture initiation on tissue culture plastic, fibroblasts were routinely subcultured on compliant silicone elastomer substrates (Excellness Biotech SA, Lausanne, Switzerland) coated with 10 μg/ml collagen type I, as previously described (Wipff et al., 2009). The culture substrate stiffness (Young's modulus) influences the behaviour of cells in general (Discher et al., 2005) and of myofibroblasts in particular (Hinz, 2009). The stiffness of normal heart muscle has been measured with AFM to vary around 10 kPa, whereas the scar of pathologically remodelled heart tissue reaches stiffness values of up to 70 kPa (Berry et al., 2006; Dean et al., 2005; Engler et al., 2008; Jacot et al., 2008). After performing a series of preliminary experiments, we adjusted the Young's modulus of our silicone substrates to 15 kPa for all experiments. This simulates the mechanical conditions of connective tissue undergoing remodelling (Goffin et al., 2006).

As culture medium, we used DMEM (Invitrogen, Basel, Switzerland), supplemented with 10% FCS (BioConcept, Allschwil, Switzerland), 2 mM L-glutamine and 100 U/ml penicillin-streptomycin (Invitrogen). Cells were used for experiments up to third passage. In selected experiments, cardiac myofibroblasts were transfected with α-SMA–EGFP (Clement et al., 2005) using the jetPEI transfection reagent according to the manufacturer's instructions (Polyplus Transfection, Chemie Brunschwig AG, Basel). For all experiments, rat cardiac fibroblasts were seeded at 3000 cells/cm^2 and cultured for four days in culture medium to reach 70% confluence at the time of assessment. To modulate $[Ca^{2+}]_i$-mediated cell activities, we applied to the experimental medium: ATP (10 nM-500 nM), EGTA (3 mM) (both Sigma), thapsigargin (0.1-1 μM) (Alexis) and 2-APB (75 μM) (Calbiochem). Rho- and ROCK-mediated cell contraction was inhibited using Y27632 (10 μM), and myosin activity was blocked with blebbistatin (50 μM) (both from Calbiochem, San Diego, CA).

Calcium imaging and microscopy

Changes in $[Ca^{2+}]_i$ were simultaneously recorded with cell contraction using live video microscopy. We used an inverted microscope (Axiovert S100TV, Carl Zeiss, Feldbach, Switzerland) equipped with a polychromatic Xenon light source (Polychrome IV, TILL Photonics, Ascheberg, Germany), high numerical aperture objectives (Plan-Neofluar 20× NA 0.50 Ph2, 40× NA 1.3 Oil Ph3 and Plan-Apochromat 63× NA 1.40 Oil Ph3; Zeiss) and a charge-coupled device camera (C4742-95 Hamamatsu, Bucher Biotech, Basel, Switzerland). Spatial resolution was 106 nm/pixel (63× objective, binning 1) and 333 nm/pixel (40× objective, binning 2). The observation chamber and objective were maintained at 37°C in a humidified atmosphere. To visualise $[Ca^{2+}]_i$ changes, myofibroblasts were incubated for 45 minutes at 37°C with 2 μM Fura-2 AM (Molecular Probes, Eugene, OR) in F-12 medium (Invitrogen) supplemented with 10% FCS, 20 mM HEPES and 0.25% pluronic acid. Cells were washed three times for 5 minutes with F-12, 10% FCS and 20 mM HEPES before recording. Samples were alternately excited at 340 nm and at 380 nm for 200 ms; pairs of fluorescence images were recorded every 5 seconds, together with one phase-contrast frame using Openlab 3.0.6 software (Bucher Biotech); frame captures were separated by less than 10 ms. An increase in $[Ca^{2+}]_i$ leads to an increase in the emitted fluorescence at 510 nm after 340 nm excitation (Em340) and a decrease in emission after 380 nm excitation (Em380). Changes in $[Ca^{2+}]_i$ levels over time were expressed in arbitrary units as $[Ca^{2+}]_i$ fluorescence ratio=Em340/Em380, calculated over regions of interest (ROIs) that included the entire cell (MetaMorph, Universal Imaging, West Chester, PA).

Analysis of myofibroblast contraction

To visualise isometric contraction, we cultured myofibroblasts on deformable 'wrinkling' silicone substrates. Substrates were prepared in homemade observation chambers with a glass coverslip bottom (#0, Karl Hecht Assistant, Altnau, Switzerland) and rendered adhesive, as described above for silicone culture substrates. Wrinkling substrates were produced with a stiffness of 15 kPa, restricting the formation of surface distortions (wrinkles) visible in phase-contrast microscopy to highly contractile myofibroblasts. The forces developed by α-SMA-negative fibroblasts were too low to produce visible surface deformations (Hinz et al., 2001).

To record contractile events in the micrometre range, we quantified the directed movement of stress-fibre-engaged particles on the dorsal cell surface. Sulfate latex beads with a diameter of 1 μm (Invitrogen) were coated with 50 μg/ml rat tail collagen type I (Sigma) or human plasma FN (Chemicon International, Temecula, CA) in Ca^{2+}- and Mg^{2+}-free PBS overnight. For experiments, beads were sonicated and incubated with cells for 45 minutes at 0.01% (w/v) dilution together with Ca^{2+}-staining medium (see above). Samples were rinsed three times to remove non-adherent beads before time-lapse video microscopy. Bead position was tracked in image sequences using a cross-correlation algorithm (MetaMorph). Analysis provided subpixel resolution with a sensitivity of 10-30 nm for 1 μm beads, depending on objective and binning (Gelles et al., 1988; Schmidt et al., 1993). Bead positions were manually identified in the first frame of a time sequence. Bead centroids were automatically determined and used as the seed point for every subsequent image in the sequence. For every cell-bound bead, one stationary reference point on the substrate surface (maximal distance of 10 μm) was tracked in every frame. Changes in reference point position were subtracted from changes in cell-bound bead position to correct for substrate drift. To distinguish directed motion from diffusion, quantitative analysis of bead motion tracks was performed using customised MATLAB (MathWorks, Natick, MA) software (supplementary material Fig. S1).

To quantify drug effects on bead movement, we calculated the ratio between the mean bead velocity before and after drug treatment, $V_{drug}/V_{control}$, and the absolute change of direction, $\Delta\theta=|\theta_{drug}-\theta_{control}|$, for every directed moving bead. All experiments were summarised in one polar plot (Fig. 4) by representing $V_{drug}/V_{control}$ as the radial coordinate (distance from origin) and $\Delta\theta$ as the angular coordinate (angle position from vertical control). Both magnitude and direction of control-bead velocities were normalised (Fig. 4, vertical vector $\mathbf{V}_{control}$ with magnitude $V_{control}$ set to 1 and $\theta_{control}$ set to 0°). Every single data point corresponds to the terminal point of the 'relative' velocity vector $\mathbf{V}_{drug}$. The average of all relative bead velocities and all relative changes of direction was represented as the vector $\overline{\mathbf{V}}_{drug}$ (Fig. 4).

Analysis of myofibroblast microcontractions and $[Ca^{2+}]_i$ changes by simultaneous AFM and fluorescence microscopy

In another approach to correlate changes in $[Ca^{2+}]_i$ with microcontractile events, we combined AFM and Ca^{2+} imaging. A Nanowizard II AFM (JPK Instruments, Berlin, Germany) was implemented on an inverted fluorescence microscope (Axiovert 200M, Zeiss). The system was equipped with a water-cooled EMCCD iXon camera (Andor Technology, Belfast, Northern Ireland) and external shutter (Uniblitz VCM-D1, Vincent Associates, Rochester, NY, USA). Cardiac myofibroblasts were observed in homemade glass-bottomed observation chambers, provided with a 15 kPa silicone layer. Changes in $[Ca^{2+}]_i$ were observed by loading cells with 10 μM of the Ca^{2+} dye Fluo4-AM (Molecular Probes). Video microscopy was performed using a 40× objective (Plan-Neofluar, 1.3 NA, Oil, Zeiss) with binning 2, 200 ms exposure time and a sampling frequency of 0.2 Hz. Micromechanical cell events were quantified using rectangular silicon nitride force probes (spring constant: k=0.030±0.003 N/m) without reflective coating. We used a 5 μm diameter borosilicate glass particle (Novascan, Ames, IA) attached to the AFM probe and ECM coated as described for 1 μm latex beads. To couple the ECM-coated AFM probe to the actin cytoskeleton, it was brought into contact with the surface of a myofibroblast, approximately 20 μm away from the cell edge. Cells were approached with an initial set point force of 250 pN, resulting in an indentation of the cell surface of 120±40 nm and a calculated bead-membrane contact area of 1-2 μm^2. Simultaneous acquisition of the

AFM signal and $[Ca^{2+}]_i$ variations was started 10 minutes after contacting the cell. Forces transmitted from the cell to the AFM probe were acquired in real-time mode. Processing of the AFM recordings and the oscillation frequency analysis of $[Ca^{2+}]_i$ and AFM signals was performed using MATLAB (MathWorks).

Immunofluorescence, transfection and antibodies

For immunofluorescence, cells were fixed for 10 minutes with 3% paraformaldehyde in PBS. We applied primary antibodies directed against: α-SMA (mouse IgG2a, SM-1, a kind gift of Giulio Gabbiani, University of Geneva, Switzerland); vinculin (mouse IgG1) and FN (rabbit) (Sigma); vimentin (mouse IgG1) and desmin (mouse IgG1) (DAKO, Baar, Switzerland); von Willebrand factor (rabbit), PECAM-1 (rabbit) and VE-cadherin (goat) (Santa Cruz Biotechnologies). As secondary antibodies, we used anti-mouse IgG2a-Alexa-Fluor-647 and anti-rabbit-Alexa-Fluor-647 (Molecular Probes); anti-mouse IgG1-FITC and IgG2a-FITC, IgG1-TRITC (Southern Biotechnology, Birmingham, AL); and anti-rabbit-FITC (Sigma). Alexa-Fluor-488-phalloidin and Alexa-Fluor-350-phalloidin (Molecular Probes) were used to visualise F-actin, and nuclei were stained with DAPI (Fluka, Buchs, Switzerland). Confocal still images were acquired using an oil immersion objective (40×, NA 1.25; Leica), mounted on an inverted confocal microscope (DM RXA2, with a laser-scanning confocal head TCS SP2 AOBS, Leica). Figures were assembled with Adobe Photoshop CS3.

Statistical analysis

All mean values are presented ± s.d. and error bars in graphs indicate s.d.

Josiane Smith-Clerc is acknowledged for excellent technical assistance and Annik Hoffmann for experimental help. We thank the staff of the BioImaging and Optics platform of the EPFL and Pam Arora in the Matrix Dynamics group for providing imaging facilities and training. Jean-Marc Vesin and Laurent Uldry from the Laboratory of Signal Processing and Cyril Castella (all EPFL) are acknowledged for stimulating discussions. We are grateful to Christopher A. McCulloch, Giulio Gabbiani and James J. Tomasek for critically reading the manuscript, expert advice and providing reagents. This work was supported by grants from the Swiss National Science Foundation (#3100A0-113733/1), from the GEBERT RÜF STIFTUNG, from the Novartis Science Foundation and from the Connaught Funding Program (all to B.H.).

Supplementary material available online at
http://jcs.biologists.org/cgi/content/full/123/10/1751/DC1

References

Arora, P. D., Bibby, K. J. and McCulloch, C. A. (1994). Slow oscillations of free intracellular calcium ion concentration in human fibroblasts responding to mechanical stretch. *J. Cell Physiol.* **161**, 187-200.

Berry, M. F., Engler, A. J., Woo, Y. J., Pirolli, T. J., Bish, L. T., Jayasankar, V., Morine, K. J., Gardner, T. J., Discher, D. E. and Sweeney, H. L. (2006). Mesenchymal stem cell injection after myocardial infarction improves myocardial compliance. *Am. J. Physiol. Heart Circ. Physiol.* **290**, H2196-H2203.

Bootman, M. D., Collins, T. J., Mackenzie, L., Roderick, H. L., Berridge, M. J. and Peppiatt, C. M. (2002). 2-aminoethoxydiphenyl borate (2-APB) is a reliable blocker of store-operated Ca^{2+} entry but an inconsistent inhibitor of InsP3-induced Ca^{2+} release. *FASEB J.* **16**, 1145-1150.

Cai, Y., Biais, N., Giannone, G., Tanase, M., Jiang, G., Hofman, J. M., Wiggins, C. H., Silberzan, P., Buguin, A., Ladoux, B. et al. (2006). Nonmuscle myosin IIA-dependent force inhibits cell spreading and drives F-actin flow. *Biophys. J.* **91**, 3907-3920.

Chen, J. B., Tao, R., Sun, H. Y., Tse, H. F., Lau, C. P. and Li, G. R. (2010). Multiple Ca^{2+} signaling pathways regulate intracellular Ca^{2+} activity in human cardiac fibroblasts. *J. Cell Physiol.* **223**, 68-75.

Clement, S., Hinz, B., Dugina, V., Gabbiani, G. and Chaponnier, C. (2005). The N-terminal Ac-EEED sequence plays a role in {alpha}-smooth-muscle actin incorporation into stress fibers. *J. Cell Sci.* **118**, 1395-1404.

Dean, R. G., Balding, L. C., Candido, R., Burns, W. C., Cao, Z., Twigg, S. M. and Burrell, L. M. (2005). Connective tissue growth factor and cardiac fibrosis after myocardial infarction. *J. Histochem. Cytochem.* **53**, 1245-1256.

Diliberto, P. A., Krishna, S., Kwon, S. and Herman, B. (1994). Isoform-specific induction of nuclear free calcium oscillations by platelet-derived growth factor. *J. Biol. Chem.* **269**, 26349-26357.

Discher, D. E., Janmey, P. and Wang, Y. L. (2005). Tissue cells feel and respond to the stiffness of their substrate. *Science* **310**, 1139-1143.

Dugina, V., Zwaenepoel, I., Gabbiani, G., Clement, S. and Chaponnier, C. (2009). {beta}- and {gamma}-cytoplasmic actins display distinct distribution and functional diversity. *J. Cell Sci.* **122**, 2980-2988.

Engler, A. J., Carag-Krieger, C., Johnson, C. P., Raab, M., Tang, H. Y., Speicher, D. W., Sanger, J. W., Sanger, J. M. and Discher, D. E. (2008). Embryonic cardiomyocytes beat best on a matrix with heart-like elasticity: scar-like rigidity inhibits beating. *J. Cell Sci.* **121**, 3794-3802.

Follonier, L., Schaub, S., Meister, J. J. and Hinz, B. (2008). Myofibroblast communication is controlled by intercellular mechanical coupling. *J. Cell Sci.* **121**, 3305-3316.

Furuya, K., Sokabe, M. and Furuya, S. (2005). Characteristics of subepithelial fibroblasts as a mechano-sensor in the intestine: cell-shape-dependent ATP release and P2Y1 signaling. *J. Cell Sci.* **118**, 3289-3304.

Gelles, J., Schnapp, B. J. and Sheetz, M. P. (1988). Tracking kinesin-driven movements with nanometre-scale precision. *Nature* **331**, 450-453.

Giannone, G., Dubin-Thaler, B. J., Dobereiner, H. G., Kieffer, N., Bresnick, A. R. and Sheetz, M. P. (2004). Periodic lamellipodial contractions correlate with rearward actin waves. *Cell* **116**, 431-443.

Goffin, J. M., Pittet, P., Csucs, G., Lussi, J. W., Meister, J. J. and Hinz, B. (2006). Focal adhesion size controls tension-dependent recruitment of alpha-smooth muscle actin to stress fibers. *J. Cell Biol.* **172**, 259-268.

Goto, T., Yanaga, F. and Ohtsuki, I. (1998). Studies on the endothelin-1-induced contraction of rat granulation tissue pouch mediated by myofibroblasts. *Biochim. Biophys. Acta* **1405**, 55-66.

Grierson, J. P. and Meldolesi, J. (1995). Shear stress-induced [Ca2+]i transients and oscillations in mouse fibroblasts are mediated by endogenously released ATP. *J. Biol. Chem.* **270**, 4451-4456.

Harks, E. G., Scheenen, W. J., Peters, P. H., van Zoelen, E. J. and Theuvenet, A. P. (2003). Prostaglandin F2 alpha induces unsynchronized intracellular calcium oscillations in monolayers of gap junctionally coupled NRK fibroblasts. *Pflugers Arch.* **447**, 78-86.

Harootunian, A. T., Kao, J. P., Paranjape, S. and Tsien, R. Y. (1991). Generation of calcium oscillations in fibroblasts by positive feedback between calcium and IP3. *Science* **251**, 75-78.

Hinz, B. (2009). The myofibroblast: Paradigm for a mechanically active cell. *J. Biomech.* **43**, 146-155.

Hinz, B., Celetta, G., Tomasek, J. J., Gabbiani, G. and Chaponnier, C. (2001). Alpha-smooth muscle actin expression upregulates fibroblast contractile activity. *Mol. Biol. Cell* **12**, 2730-2741.

Hinz, B., Dugina, V., Ballestrem, C., Wehrle-Haller, B. and Chaponnier, C. (2003). Alpha-smooth muscle actin is crucial for focal adhesion maturation in myofibroblasts. *Mol. Biol. Cell* **14**, 2508-2519.

Hotulainen, P. and Lappalainen, P. (2006). Stress fibers are generated by two distinct actin assembly mechanisms in motile cells. *J. Cell Biol.* **173**, 383-394.

Jacot, J. G., McCulloch, A. D. and Omens, J. H. (2008). Substrate stiffness affects the functional maturation of neonatal rat ventricular myocytes. *Biophys. J.* **95**, 3479-3487.

Kahan, A., Coghlan, G. and McLaughlin, V. (2009). Cardiac complications of systemic sclerosis. *Rheumatology* **48**, iii45-iii48.

Kamm, K. E. and Stull, J. T. (1989). Regulation of smooth muscle contractile elements by second messengers. *Annu. Rev. Physiol.* **51**, 299-313.

Katoh, K., Kano, Y., Amano, M., Kaibuchi, K. and Fujiwara, K. (2001a). Stress fiber organization regulated by MLCK and Rho-kinase in cultured human fibroblasts. *Am. J. Physiol. Cell Physiol.* **280**, C1669-C1679.

Katoh, K., Kano, Y., Amano, M., Onishi, H., Kaibuchi, K. and Fujiwara, K. (2001b). Rho-kinase-mediated contraction of isolated stress fibers. *J. Cell Biol.* **153**, 569-584.

Lazzerini, P. E., Capecchi, P. L., Guideri, F., Acampa, M., Galeazzi, M. and Laghi Pasini, F. (2006). Connective tissue diseases and cardiac rhythm disorders: an overview. *Autoimmun. Rev.* **5**, 306-313.

Levinson, H., Moyer, K. E., Saggers, G. C. and Ehrlich, H. P. (2004). Calmodulin-myosin light chain kinase inhibition changes fibroblast-populated collagen lattice contraction, cell migration, focal adhesion formation, and wound contraction. *Wound Repair Regen.* **12**, 505-511.

Liang, W., McDonald, P., McManus, B., van Breemen, C. and Wang, X. (2003). Histamine-induced Ca(2+) signaling in human valvular myofibroblasts. *J. Mol. Cell. Cardiol.* **35**, 379-388.

Meshel, A. S., Wei, Q., Adelstein, R. S. and Sheetz, M. P. (2005). Basic mechanism of three-dimensional collagen fibre transport by fibroblasts. *Nat. Cell Biol.* **7**, 157-164.

Munevar, S., Wang, Y. L. and Dembo, M. (2004). Regulation of mechanical interactions between fibroblasts and the substratum by stretch-activated Ca^{2+} entry. *J. Cell Sci.* **117**, 85-92.

Parizi, M., Howard, E. W. and Tomasek, J. J. (2000). Regulation of LPA-promoted myofibroblast contraction: role of Rho, myosin light chain kinase, and myosin light chain phosphatase. *Exp. Cell Res.* **254**, 210-220.

Pellegrin, S. and Mellor, H. (2007). Actin stress fibres. *J. Cell Sci.* **120**, 3491-3499.

Pelling, A. E., Veraitch, F. S., Pui-Kei Chu, C., Nicholls, B. M., Hemsley, A. L., Mason, C. and Horton, M. A. (2007). Mapping correlated membrane pulsations and fluctuations in human cells. *J. Mol. Recognit.* **20**, 467-475.

Petroll, W. M., Ma, L., Kim, A., Ly, L. and Vishwanath, M. (2008). Dynamic assessment of fibroblast mechanical activity during Rac-induced cell spreading in 3-D culture. *J. Cell Physiol.* **217**, 162-171.

Pletjushkina, O. J., Rajfur, Z., Pomorski, P., Oliver, T. N., Vasiliev, J. M. and Jacobson, K. A. (2001). Induction of cortical oscillations in spreading cells by depolymerization of microtubules. *Cell Motil. Cytoskeleton* **48**, 235-244.

Raizman, J. E., Komljenovic, J., Chang, R., Deng, C., Bedosky, K. M., Rattan, S. G., Cunnington, R. H., Freed, D. H. and Dixon, I. M. (2007). The participation of the Na^+-Ca^{2+} exchanger in primary cardiac myofibroblast migration, contraction, and proliferation. *J. Cell. Physiol.* **213**, 540-551.

Ridefelt, P., Yokote, K., Claesson-Welsh, L. and Siegbahn, A. (1995). PDGF-BB triggered cytoplasmic calcium responses in cells with endogenous or stably transfected PDGF beta-receptors. *Growth Factors* **12**, 191-201.

Journal of Cell Science

Ronnov-Jessen, L. and Petersen, O. W. (1996). A function for filamentous alpha-smooth muscle actin: retardation of motility in fibroblasts. *J. Cell Biol.* **134**, 67-80.
Salbreux, G., Joanny, J. F., Prost, J. and Pullarkat, P. (2007). Shape oscillations of non-adhering fibroblast cells. *Phys. Biol.* **4**, 268-284.
Schmidt, C. E., Horwitz, A. F., Lauffenburger, D. A. and Sheetz, M. P. (1993). Integrin-cytoskeletal interactions in migrating fibroblasts are dynamic, asymmetric, and regulated. *J. Cell Biol.* **4**, 977-991.
Sheetz, M. P., Turney, S., Qian, H. and Elson, E. L. (1989). Nanometre-level analysis demonstrates that lipid flow does not drive membrane glycoprotein movements. *Nature* **340**, 284-288.
Tamariz, E. and Grinnell, F. (2002). Modulation of fibroblast morphology and adhesion during collagen matrix remodeling. *Mol. Biol. Cell* **13**, 3915-3929.
Tomasek, J. J., Gabbiani, G., Hinz, B., Chaponnier, C. and Brown, R. A. (2002). Myofibroblasts and mechano-regulation of connective tissue remodelling. *Nat. Rev. Mol. Cell Biol.* **3**, 349-363.
Tomasek, J. J., Vaughan, M. B., Kropp, B. P., Gabbiani, G., Martin, M. D., Haaksma, C. J. and Hinz, B. (2006). Contraction of myofibroblasts in granulation tissue is dependent on Rho/Rho kinase/myosin light chain phosphatase activity. *Wound Repair Regen.* **14**, 313-320.
Totsukawa, G., Yamakita, Y., Yamashiro, S., Hartshorne, D. J., Sasaki, Y. and Matsumura, F. (2000). Distinct roles of ROCK (Rho-kinase) and MLCK in spatial regulation of MLC phosphorylation for assembly of stress fibers and focal adhesions in 3T3 fibroblasts. *J. Cell Biol.* **150**, 797-806.
Uhlen, P., Burch, P. M., Zito, C. I., Estrada, M., Ehrlich, B. E. and Bennett, A. M. (2006). Gain-of-function/Noonan syndrome SHP-2/Ptpn11 mutants enhance calcium oscillations and impair NFAT signaling. *Proc. Natl. Acad. Sci. USA* **103**, 2160-2165.
van Rossum, D. B., Patterson, R. L., Ma, H. T. and Gill, D. L. (2000). Ca^{2+} entry mediated by store depletion, S-nitrosylation, and TRP3 channels. Comparison of coupling and function. *J. Biol. Chem.* **275**, 28562-28568.
Vogel, V. and Sheetz, M. P. (2009). Cell fate regulation by coupling mechanical cycles to biochemical signaling pathways. *Curr. Opin. Cell Biol.* **21**, 38-46.
Wang, J., Zohar, R. and McCulloch, C. A. (2006). Multiple roles of alpha-smooth muscle actin in mechanotransduction. *Exp. Cell Res.* **312**, 205-214.
Wipff, P. J. and Hinz, B. (2008). Integrins and the activation of latent transforming growth factor beta1-an intimate relationship. *Eur. J. Cell Biol.* **87**, 601-615.
Wipff, P. J., Majd, H., Acharya, C., Buscemi, L., Meister, J. J. and Hinz, B. (2009). The covalent attachment of adhesion molecules to silicone membranes for cell stretching applications. *Biomaterials* **30**, 1781-1789.
Wrobel, L. K., Fray, T. R., Molloy, J. E., Adams, J. J., Armitage, M. P. and Sparrow, J. C. (2002). Contractility of single human dermal myofibroblasts and fibroblasts. *Cell Motil. Cytoskeleton* **52**, 82-90.
Wu, C., Sui, G. P. and Fry, C. H. (2004). Purinergic regulation of guinea pig suburothelial myofibroblasts. *J. Physiol.* **559**, 231-243.
Wynn, T. A. (2008). Cellular and molecular mechanisms of fibrosis. *J. Pathol.* **214**, 199-210.